Journal of Solid State Chemistry 182 (2009) 240–245

Contents lists available at ScienceDirect

Journal of Solid State Chemistry

journal homepage: www.elsevier.com/locate/jssc

Structure and high-temperature thermoelectric properties of $SrAl_2Si_2$

Susan M. Kauzlarich [a,*], Cathie L. Condron [a], Jonathan K. Wassei [a], Teruyuki Ikeda [b], G. Jeffrey Snyder [b]

[a] Department of Chemistry, University of California, One Shields Avenue, Davis, CA 95616, USA
[b] Materials Science, California Institute of Technology, 1200 California Boulevard, Pasadena, CA 91125, USA

ARTICLE INFO

Article history:
Received 6 August 2008
Received in revised form
17 September 2008
Accepted 20 September 2008
Available online 29 October 2008

Keywords:
$CaAl_2Si_2$
Zintl
Thermoelectric
High-temperature thermoelectric material
Thermal conductivity
ZT
Silicides
Aluminum silicide
Strontium
Ternary phase

ABSTRACT

Single crystals of $SrAl_2Si_2$ were synthesized by reaction of the elements in an aluminum flux at 1000 °C. $SrAl_2Si_2$ is isostructural to $CaAl_2Si_2$ and crystallizes in the hexagonal space group P–3m1 (90 K, $a = 4.1834$ (2), $c = 7.4104$ (2) Å, $Z = 1$, $R1 = 0.0156$, w$R2 = 0.0308$). Thermal analysis shows that the compound melts at ~1020 °C. Low-temperature resistivity on single crystals along the c-axis shows metallic behavior with room temperature resistivity value of ~7.5 mΩ cm. High-temperature Seebeck, resistivity, and thermal conductivity measurements were made on hot-pressed pellets. The Seebeck coefficient shows negative values in entire temperature range decreasing from $\sim -78\ \mu V\ K^{-1}$ at room temperature to $-34\ \mu V\ K^{-1}$ at 1173 K. Seebeck coefficients are negative indicating n-type behavior; however, the temperature dependence is consistent with contribution from minority p-type carriers as well. The lattice contribution to the thermal conductivity is higher than for clathrate structures containing Al and Si, approximately 50 mW cm^{-1} K, and contributes to the overall low zT for this compound.

1. Introduction

Thermoelectric materials have been studied for many years due to their unique and useful properties [1]. More recently, lightweight thermoelectric materials have been studied more aggressively because decreasing the weight of the material can open doors to many other applications. Preliminary results on the $Ba_8Al_{14}Si_{31}$ compound, a type I clathrate phase, provided incentive for further investigation of these clathrate light element containing structures [2,3]. An investigation to produce the $Sr_8Al_{16}Si_{30}$ clathrate phase via Al flux reaction revealed that a 1:2:2 crystal phase was produced as the major phase regardless of composition or conditions.

Ternary Sr–Al–Si system has produced the clathrate type I structure by arc melting the appropriate elemental combinations [4]. Ternary hydrides of Sr–Al–Si have also been reported. SrAlSiH crystallizes in a layered structure ($P3m1$), where Al and Si are in an ordered hexagonal sheet with the hydrogen capping the Al on one side only [5]. The layers are interspersed with Si atoms. The $AAl_{2-x}Si_x$ ($x = 1$, A = Ca, Sr) phases [6–8] crystallize as the AlB_2-type structure ($P6/mmm$) and show superconductivity at 7.8 K, and 4.2 K [6,9]. These phases have been extensively studied in relation with the superconductor MgB_2, although there is some controversy over the intrinsic nature of the superconductivity [8]. The Ba phase has been shown to be a superconductor when slightly off composition, with a $T_c = 2.8$ K. The 1-2-2 structure for Sr–Al–Si has not yet been reported, but it might be expected be either the α-$BaCu_2S_2$-type ($Pnma$), similar to $BaAl_2Si_2$, or the $CaAl_2Si_2$ structure-type (P–3m1). The electrical properties of single crystal $BaAl_2Si_2$ and $CaAl_2Si_2$ have been studied [10,11]. $BaAl_2Si_2$ shows metallic conductivity and Pauli paramagnetic behavior (300–2 K) [10]. Transport properties of $CaAl_2Si_2$ show both electrons (300–150 K) and holes (below 150 K) contribute to the metallic conductivity [11].

In addition to the alkaline earth aluminum silicides of the formula 1-2-2, rare earth metal cations with 2+ valence can also be prepared, $LnAl_2Si_2$, Ln = Eu, Yb [12–14]. These compounds crystallize in the $CaAl_2Si_2$-type structure and show metamagnetic transitions at low temperatures. Early measurements on $YbAl_2Si_2$ were interpreted as typical behavior of an intermediate-valent compound [12], however; more recent measurements do not support this conclusion [14].

We report the synthesis, structure, and transport properties of $SrAl_2Si_2$, along with the high-temperature thermoelectric properties.

2. Experimental section

2.1. Synthesis

Starting materials for the preparation of $SrAl_2Si_2$ were Sr (ALFA AESAR, 99%), Si (AESAR, 99.999%), and Al (Matheson Colemen and

* Corresponding author. Fax: +1 530 752 8995.
E-mail address: smkauzlarich@ucdavis.edu (S.M. Kauzlarich).

0022-4596/$ - see front matter © 2008 Elsevier Inc. All rights reserved.
doi:10.1016/j.jssc.2008.09.028

Bell 99.6%). All preparations were performed in nitrogen-filled dry box with water levels less than 1 ppm. Single-crystal samples were grown utilizing the high-temperature metallic solution growth method [15] with the optimized atomic ratio of the elements of 8:30:70 (Sr:Si:Al) scaled to 1 g of Al.

2.2. Microprobe analysis

Single crystals of $SrAl_2Si_2$ were obtained from several different reactions, mounted in epoxy and polished for subsequent analyses. The samples were then placed in a Cameca SX-100 electron microprobe equipped with five wavelength-dispersive spectrometers. The microprobe was operated at 10 nA current with a 20 keV accelerating potential. Net elemental intensities for Al and Si were determined with respect to pure elemental calibration standards. $SrBaNb_4O_{10}$ was used as the standard to determine the net elemental intensities for Sr. Totals for all analysis were 100%. The elemental stoichiometry was quantitatively determined to be $Sr_{1.00(3)}Al_{2.00(2)}Si_{1.96(4)}$. The compositions were homogeneous within one crystal and, within standard deviation, identical compared with random crystals from different reactions.

2.3. X-ray powder diffraction

X-Ray powder diffraction data for $SrAl_2Si_2$ were collected with a Sintag PAD-V employing Cu$K\alpha$ radiation. Data acquisition was performed with WinAcq software. Sample analyses were performed using the RIETICA software package.

2.4. Single crystal X-ray diffraction

The single-crystal X-ray diffraction data for $SrAl_2Si_2$ were collected at ~90 K using a Bruker SMART 1000 CCD diffractometer employing graphite-monochromatized Mo$K\alpha$ radiation ($\lambda = 0.71069$ Å). Data were collected in full sphere with 0.3° scans in ω, and exposure time of 20 s per frame. Lorentz and polarization effects were corrected for using the SAINT program, and absorption corrections were based on fitting a function to the empirical transmission surface as sampled by multiple equivalent reflections (program SADABS) [16]. The structure solution was obtained by direct methods and refined by full-matrix least-squares refinement against F_0^2 using the SHELXTL 6.10 package (see Table 1) [16].

2.5. Thermal analysis

A Netzsch Thermal Analysis STA 409 STA was used to evaluate the thermal properties between 25 and 1500 °C. After a baseline was established, several crystals ground into a powder (40–60 mg) was placed in alumina crucibles and heated under argon at 10 K min^{-1} with an acquisition rate of 4 pts K^{-1}.

2.6. Low-temperature resistivity of single crystals

Resistivity of $SrAl_2Si_2$ was measured on a crystal of $2 \times 0.5 \times 1$ mm^3 dimensions. Platinum wires were attached to the crystal with Epo–Tex silver epoxy. The temperature dependence of $SrAl_2Si_2$ was measured using the four-probe method over the temperature range of 300–2 K using a Quantum Design PPMS (physical properties measurement system). Two single crystals were measured from 2 to 300 K to check the reproducibility.

Table 1
Crystal data and structure refinement for $SrAl_2Si_2$..

Crystal system	Hexagonal
Space group	$P\text{–}3m1$
Lattice parameters (Å)	$a = 4.1834$ (2)
	$c = 7.4104$ (2)
Volume (Å^3)	112.313
Z	1
Density (calculated) (Mg/m^3)	2.924
Absorption coefficient (mm^{-1})	12.713
Theta range (°)	5.50–28.16
Reflections collected	1435
Independent reflections	132
Data/Restraints/Parameters	132/0/10
Goodness-of-fit on F^2	1.083
Final R indices [$I > 2$sigma(I)][a]	$R1 = 0.0156$; w$R2 = 0.0308$
R Indices (all data)	$R1 = 0.0163$; w$R2 = 0.0309$
Extinction coefficient	0.0033(12)
Largest diff. peak and hole (e. Å^{-3})	1.055 and −1.398

[a] $R1 = [\sum\|F_0|-|F_c\|]/\sum|F_0|$; $wR2 = \{[\sum w[(F_0)^2-(F_c)^2]^2]\}^{1/2}$; $w^{-1} = [\sigma^2(F_o)+(0.0471P)^2+(0.5945P)]$, where $P = [\max(F_o^2,0)+2F_c^2/3]$.

2.7. Polycrystalline properties sample preparation

In order to obtain dense samples, finely ground polycrystalline powder was hot-pressed in high-density graphite dies (POCO). A disc ~2 mm thick and 12 mm in diameter was obtained. Experimental density (calculated from measured dimensions and weight) was found to be ~95% of the theoretical density. Hot-pressing was conducted at ~124 MPa and 1173 K for 1.5 h under argon.

For electrical and thermal transport properties, the surface of the discs were polished with a #600 SiC paper. The final dimension of the discs was 1.8 mm thickness and 12 mm diameter.

2.8. Scanning electron microscopy (SEM)

For microstructural observations by SEM, the sample which was used for property measurements, the hot-pressed discs, were mechanically polished with a series of SiC papers and 0.3 μm alumina paste in water and finally with colloidal silica. Microstructures were observed using a field emission-scanning electron microscope (Carl Zeiss LEO 1550 VP) equipped with a Robinson backscattered electron (BSE) detector for its high compositional contrast capabilities. The chemical compositions of several points in each sample were measured using an energy dispersive X-ray spectrometer (EDX, INCAEnergy energy dispersion X-ray microanalysis system, Oxford Instruments). The X-ray intensities were converted to chemical compositions by ZAF method [17].

2.9. High-temperature thermoelectric properties measurements

All physical properties were measured between room temperature and 1173 K. The electrical resistivity (ρ) was measured using the van der Pauw technique with a current of 100 mA and a special high-temperature apparatus [18]. The Hall coefficient was measured in the same apparatus with a forward and reverse magnetic field value of ~10,000 G. The carrier density (n) was calculated from the Hall coefficient (R_H) assuming a scattering factor of 1.0 in a single carrier scheme, with $n = 1/R_He$, where n is the densities of charge carriers (holes), and e the charge of the electron. The Hall mobility (μ_H) was calculated from the Hall coefficient and resistivity values with $\mu_H = R_H/\rho$. The Seebeck coefficient (α) was measured using a high-temperature light pulse technique using a Chromel/Nb thermocouple up to 773 K and a W/Nb thermocouple above 600 K [19].

The thermal diffusivity was measured by a flash diffusivity technique (LFA 457, NETZSCH) [20]. The heat capacity was measured using the same instrument. The thermal conductivity (κ) was calculated from the experimental values of the heat capacity, density, and thermal diffusivity.

3. Results and discussion

Single crystals of $SrAl_2Si_2$ were prepared via an Al flux reaction. Initially, the compound was prepared with trying to make single crystals of the type I clathrate phase, $Sr_8Al_{16}Si_{30}$ via flux reaction. Different stoichiometries were explored in a systematic fashion, while the temperature scheme was kept constant, the samples were heated to 1000 °C to insure that all metals were liquids. After 10 h at this high temperature, the reaction was cooled slowly to 900 °C where the reaction vessel was removed from the furnace, inverted and centrifuged to remove any molten material. All of the reactions resulted in crystals of $SrAl_2Si_2$. Microprobe analysis of the single crystals was consistent with the formula as written.

Single crystal and powder X-ray diffraction show that the structure is the $CaAl_2Si_2$ structure type, as shown in Fig. 1. The single crystal X-ray diffraction results are summarized in Table 1 and positional parameters in Table 2. Al and Si were denoted based on the assignments given for $CaAl_2Si_2$. This structure type is well studied as it is fairly scarce compared with compounds of the $ThCr_2Si_2$ structure, and its formation is tied to certain conditions such as the number of valence electrons is limited to 16 [21,22]. It is a layered structure in which every atom in the layer is four-coordinate and each element is site specific with alternating Al–Si atoms. This site specificity of this structure type is well-known and has been discussed in detail [21–25]. There are two fairly similar Al–Si bond distances of 2.5203 (5) and 2.598 (2) Å. Powder diffraction of the ground crystals is shown in Fig. 2 and is in good agreement with the expected structure.

TG/DSC measurements in Fig. 3 show a small endotherm at about 550 °C (heating) that is attributed to a small amount of Al–Si eutectic that is present from the flux. There is a large endotherm at 1020 °C which is attributed to the main phase melting with a pre-endotherm at about 1000 °C. The cooling cycle shows the corresponding exotherm of recrystallization of the major phase with several small exotherms. The inset shows the powder diffraction pattern after the TG/DSC cycle and indicates small impurities being present in the final powder diffraction pattern, indicating that this phase melts incongruently, or is sensitive to oxygen (even very small amounts) at elevated temperatures.

Fig. 4 shows the low-temperature resistivity of two crystals from different reactions from 300 to 5 K with resistivity measured along the long axis of the crystal, the *c*-axis. The temperature dependence is reminiscent of that observed for $CaAl_2Si_2$ single crystals [11], with a more pronounced saturation at about 150 K. The room temperature resistivity is larger (7–8 mΩ cm) than that observed for $CaAl_2Si_2$ (0.5–2 mΩ cm) [11], but this may be due to cracks in the crystals as the samples are fairly brittle. $CaAl_2Si_2$ has been classified as a semimetal with the dominant carriers being holes below 150 K and electrons above that temperature [11]. The behavior of the resistivity of $SrAl_2Si_2$ is very similar and we speculate that the transport properties would also involve both electrons and holes.

Figs. 5 and 6 show the high-temperature electrical resistivity and Seebeck coefficient of polycrystalline $SrAl_2Si_2$ measured as functions of temperature, respectively. The electrical resistivity decreases from 0.95 mΩ cm at room temperature to 0.6 mΩ cm at 1173 K with increasing temperature. This value is lower than the single crystal value and likely due to the isotropic mixture of

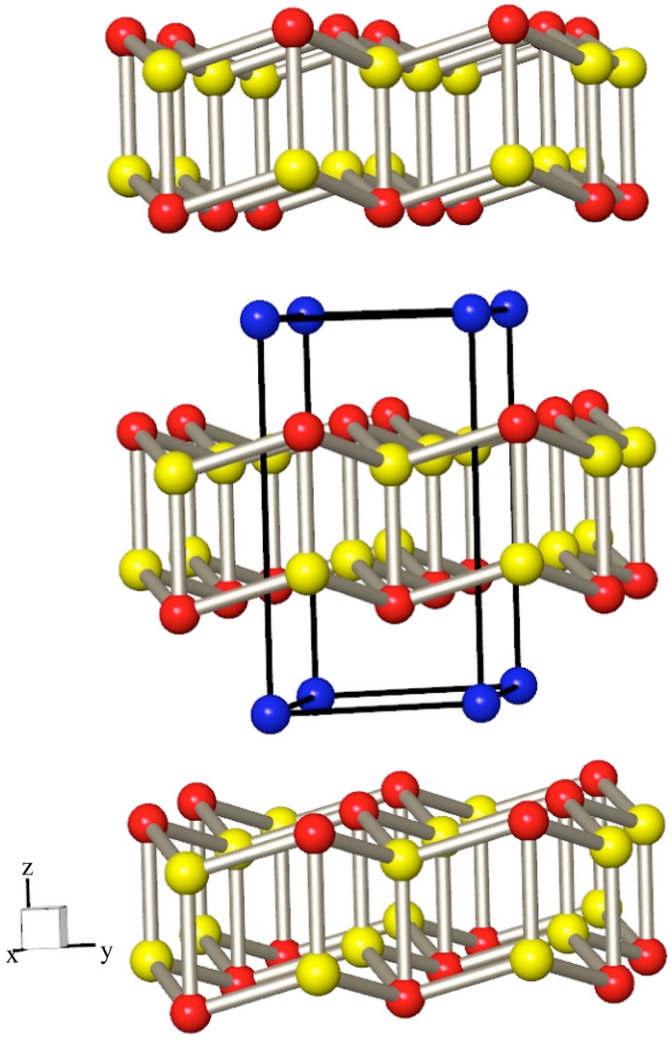

Fig. 1. Illustration of the crystal structure for $SrAl_2Si_2$. Red = Si, Yellow = Al, Blue = Sr. (For interpretation of the references to color in this figure legend, the reader is referred to the web version of this article.)

Table 2
Atomic coordinates and equivalent isotropic displacement parameters (U_{eq})[a] for $SrAl_2Si_2$..

Atom	*x*	*y*	*z*	U_{eq} (Å^2)	Occ.
Sr	0	0	0	0.0047 (2)	1
Al	0.3333	0.6667	0.6267 (2)	0.0055 (3)	1
Si	0.3333	0.6667	0.2761 (2)	0.0055 (3)	1

[a] U_{eq} is defined as one third of the trace of the orthogonalized U^{ij} tensor.

crystallites. While only one direction was measured for the single crystal samples of $SrAl_2Si_2$ reported here (along the long axis of the crystal, the *c* planes), the perpendicular direction for $CaAl_2Si_2$ is shown to have a significantly lower resistivity value [11]. The magnitude of the resistivity of the pressed pellet would be consistent with a low resistance pathway similar to that reported for $CaAl_2Si_2$. This type of electrical conductivity is typically due to the thermal activation of carriers but the relatively gradual decrease in resistivity implies an activation energy (or band gap/2) of approximately 0.02 eV.

The Seebeck coefficient shows negative value in the entire temperature range examined. The absolute value of the Seebeck coefficient decreases from ~78 μV K^{-1} at room temperature to 34 μV K^{-1} at 1173 K with increasing temperature. The temperature

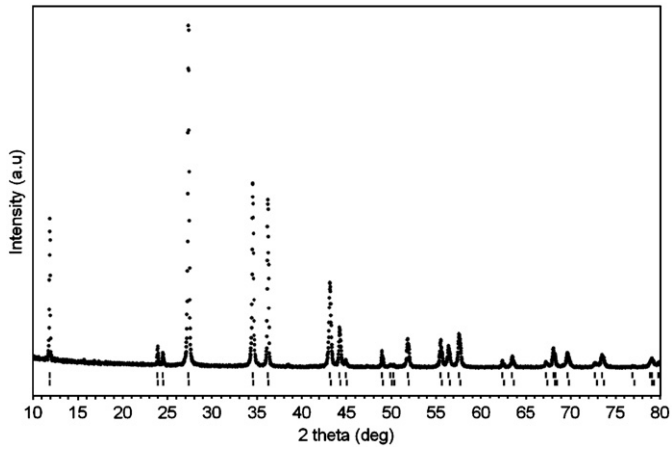

Fig. 2. X-ray powder diffraction pattern for $SrAl_2Si_2$. Experimental data points are shown as black dots, and the calculated peak positions are shown as black ticks.

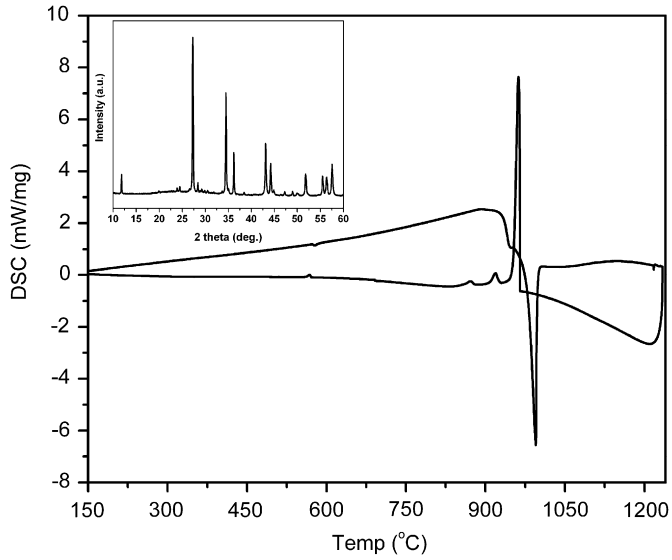

Fig. 3. DSC traces for $SrAl_2Si_2$. Inset shows the powder X-ray diffraction pattern for the sample after DSC.

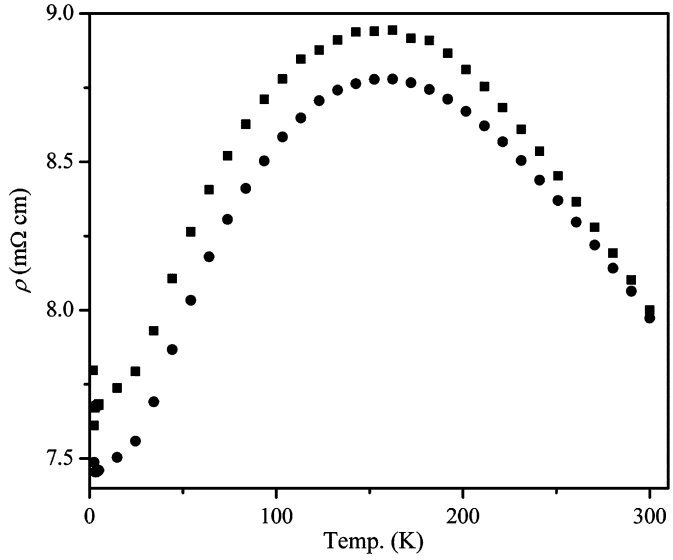

Fig. 4. Low-temperature resistivity for single crystal $SrAl_2Si_2$ measured along the *c*-axis. Two single crystals were measured to check the reproducibility.

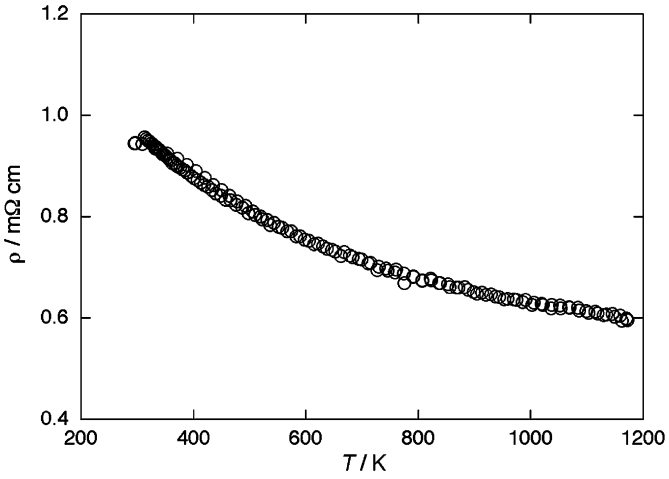

Fig. 5. Electrical resistivity ρ of polycrystalline $SrAl_2Si_2$ at high temperature.

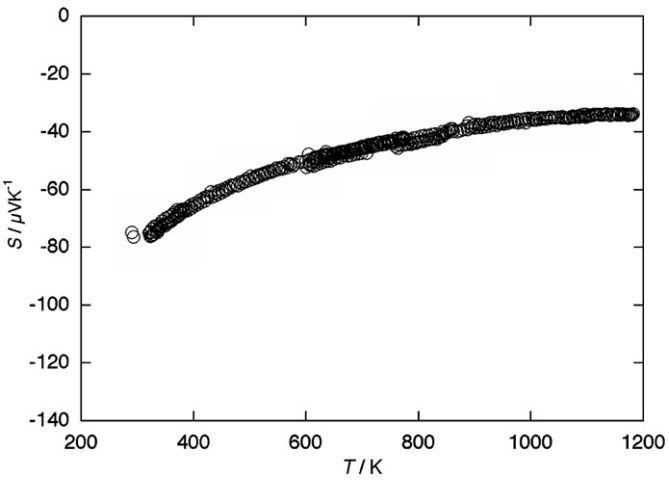

Fig. 6. Seebeck coefficient S of polycrystalline $SrAl_2Si_2$ as a function of temperature.

dependence of the resistivity and the Seebeck coefficient are typical of intrinsic semiconductors, where minority p-type carriers are excited reducing the absolute Seebeck coefficient and resistivity with increasing temperature. Thus, both n-type and p-type carriers are operative in $SrAl_2Si_2$. This character is also seen in $CaAl_2Si_2$ [11].

Fig. 7(a) and (b) shows the thermal conductivity and specific heat capacity as a function of temperature, respectively. Fig. 7(b) also shows the theoretical specific heat 0.6306 $Jg^{-1}K^{-1}$, calculated from the Dulong–Petit law $3R/\bar{M}$, where R is the gas constant measured in heat per Kelvin per mole and $\bar{M}$ is the average molar mass. The C_P data are reasonable since it increases with increasing temperature and approaches asymptotically to the Dulong–Petit value at high temperatures. We should note that while the specific heat capacity measured at constant pressure should be larger than the Dulong–Petit value at high temperature, the difference between them is generally small. The thermal conductivity was calculated from the experimental thermal diffusivity, density, and specific heat capacity. The electron component of the thermal conductivity κ_{ele} was estimated using the Wiedemann–Franz law, $\kappa_{ele} = LT\rho^{-1}$, where L is the Lorentz number ($L = 2.45 \times 10^{-8}\,W\,\Omega\,K^{-2}$). The summation of lattice component and bipolar component $\kappa_{lat}+\kappa_{bip}$ was estimated using $\kappa_{lat}+\kappa_{bip} = \kappa_{tot}-\kappa_{ele}$. The increase in the $\kappa_{lat}+\kappa_{bip}$ component with increasing temperature is attributed to the bipolar term due to excitation of the minority p-type

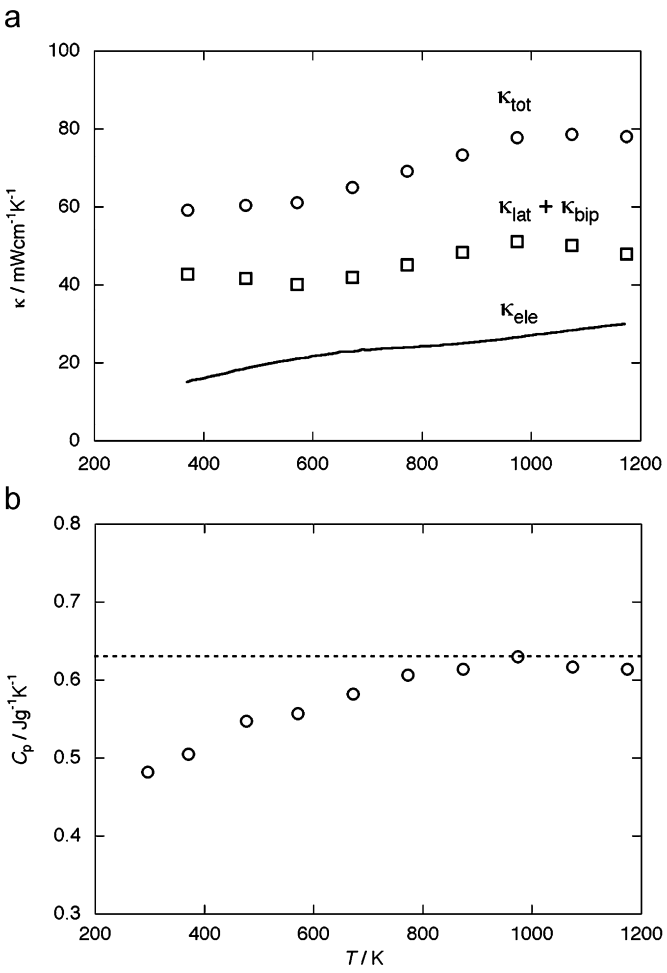

Fig. 7. Thermal conductivities κ_{tot}, κ_{ele}, and $\kappa_{lat}+\kappa_{bip}$ (a) and specific heat capacity C_P (b) of polycrystalline $SrAl_2Si_2$ as functions of temperature. The broken line in (b) shows the Dulong–Petit value for the specific heat capacity.

carriers. The lattice thermal conductivity, estimated to be about 50 mW cm^{-1} K^{-1} from the low-temperature values, is significantly larger than those of clathrates with similar chemical composition such as $Ba_{8-x}Sr_xAl_{16-x}Si_{32-y}$ [2,26] and boron-doped $Ba_8Al_{14}Si_{31}$ [27], which shows total thermal conductivities of ~20 mW cm^{-1} K^{-1} at 400 K. This is mainly because the $SrAl_2Si_2$ structure does not scatter the heat carrying phonons as well as the clathrate guest-host structure. This may be due to the strong bonding, site specificity and/or lack of disorder in the structure as there are other compounds of the $CaAl_2Si_2$ structure type that have promising thermoelectric properties such as $Yb_{1-x}Ca_xZn_2Sb_2$ which exhibits a low (~10–20 mW cm^{-1} K^{-1}) thermal conductivity [28]. Fig. 8 shows the figure of merit zT of $SrAl_2Si_2$ calculated from the experimental electrical resistivity, Seebeck coefficient, and thermal conductivity. zT is not as large enough to make a potentially useful thermoelectric material at present. It is well known that thermal conductivity can be lowered by inducing structural disorder. The presence of mixed (n- and p-type) carriers also limits the zT. For high thermoelectric efficiency, it is typically necessary to be increase or locate a larger electronic band gap to eliminate a carrier type.

4. Conclusions

Single crystals of $SrAl_2Si_2$ have been prepared via an Al flux reaction and of the $CaAl_2Si_2$ structure type. The melting point of this compound is approximately 1020 °C. Low-temperature resistivity curve is similar to that observed for single crystals of $CaAl_2Si_2$ and both n- and p-type carriers are postulated as contributing to the transport. The high-temperature Seebeck coefficient is negative, indicating n-type carriers. The temperature dependence of the Seebeck coefficient suggests additional contributions from minority p-type carriers. The lattice contribution to the thermal conductivity is higher than that observed for other Al–Si containing ternary phases of the clathrate I structure type.

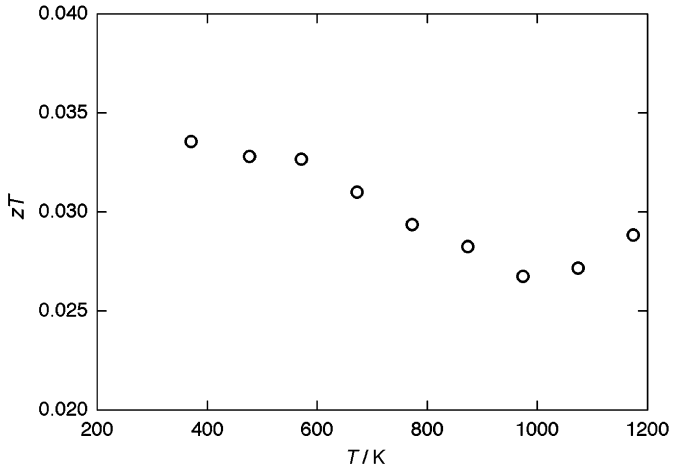

Fig. 8. Figure of merit zT ($= S^2/\rho\kappa$) of polycrystalline $SrAl_2Si_2$ calculated from electrical resistivity ρ, Seebeck coefficient S, and thermal conductivity κ measured as a function of temperature.

5. Supporting information available

Further details of the crystal structure investigation can be obtained from the Fachinformationszentrum Karlsruhe, 76344 Eggenstein-Leopoldshafen, Germany, (fax: (49) 7247-808-666; e-mail: crysdata@fiz.karlsruhe.de) on quoting the depository number CSD 419886.

Acknowledgments

The authors gratefully acknowledge Dr. Alexandra Navrotsky (Department of Chemistry and Thermochemistry Facility and NEAT ORU, University of California Davis) for use of the Scintag powder diffractometer. This work was supported by the National Science Foundation (Grant DMR-0600742), and CLC acknowledges a Tyco Electronics Foundation Fellowship in functional materials. Financial support for Caltech came from NASA-GRC NRA.

References

[1] G.J. Snyder, E.S. Toberer, Nature Mater. 7 (2008) 105.
[2] C.L. Condron, S.M. Kauzlarich, F. Gascoin, G.J. Snyder, Chem. Mater. 18 (2006) 4939.
[3] C.L. Condron, J. Martin, G.S. Nolas, P.M.B. Piccoli, A.J. Schultz, S.M. Kauzlarich, Inorg. Chem. 45 (2006) 9381.
[4] B. Eisenmann, H. Schaefer, R. Zagler, J. Less-Comm. Met. 118 (1986) 43.
[5] M.H. Lee, O.F. Sankey, T. Björling, D. Moser, D. Noréus, S.F. Parker, U. Häussermann, Inorg. Chem. 46 (2007) 6987.
[6] M. Imai, E.-H.S. Sadki, H. Abe, K. Nishida, T. Kimura, T. Sato, K. Hirata, H. Kitazawa, Phys. Rev. B: Condens. Matter 68 (2003) 064512.
[7] T. Nakagawa, M. Tokunaga, T. Tamegai, Sci. Technol. Adv. Mater. 7 (2006) S108.
[8] S. Yamanaka, T. Otsuki, T. Ide, H. Fukuoka, R. Kumashiro, T. Rachi, K. Tanigaki, F. Guo, K. Kobayashi, Physica C 451 (2007) 19.
[9] Y.K. Kuo, K.M. Sivakumar, J.I. Tasi, C.S. Lue, J.W. Huang, S.Y. Wang, D. Varshney, N. Kaurav, R.K. Singh, J. Phys.: Condens. Matter 19 (2007) 176206.

[10] C.L. Condron, H. Hope, P.M.B. Piccoli, A.J. Schultz, S.M. Kauzlarich, Inorg. Chem. 46 (2007) 4523.
[11] M. Imai, H. Abe, K. Yamada, Inorg. Chem. 43 (2004) 5186.
[12] C. Kranenberg, D. Johrendt, A. Mewis, R. Pottgen, G. Kotzyba, C. Rosenhahn, B.D. Mosel, Solid State Sci. 2 (2000) 215.
[13] C. Kranenberg, D. Johrendt, A. Mewis, Z. Anorg. Allg. Chem. 625 (1999) 1787.
[14] S. Bobev, P.H. Tobash, V. Fritsch, J.D. Thompson, M.F. Hundley, J.L. Sarrao, Z. Fisk, J. Solid State Chem. 178 (2005) 2091.
[15] P.C. Canfield, Z. Fisk, Philos. Mag. B 65 (1992) 1117.
[16] G.M. Sheldrick, Bruker Analytical X-ray Systems, XRD Single-Crystal Software, Madison, WI, 1999.
[17] Z.B. Alfassi, Nondestructive Elemental Analysis, Blackwell Publishing, Malden, MA, 2001.
[18] J.A. McCormack, J.P. Fleurial, Mater. Res. Soc. Symp. Proc. 234 (1991) 135.
[19] C. Wood, D. Zoltan, G. Stapfer, Rev. Sci. Instrum. 56 (1985) 719.
[20] J.W. Vandersande, C. Wood, A. Zoltan, D. Whittenberger, Therm. Conductivity 19 (1988) 445.
[21] C. Zheng, R. Hoffmann, R. Nesper, H.-G. von Schnering, J. Am. Chem. Soc. 108 (1986) 1876.
[22] J.K. Burdett, G.J. Miller, Chem. Mater. 2 (1990) 12.
[23] R. Ramirez, R. Nesper, H.G. Von Schnering, M.C. Bohm, Z. Naturforsch., A: Phys. Sci. 42 (1987) 670.
[24] Z.N. Chong, R. Hoffmann, J. Solid State Chem. 72 (1988) 58.
[25] A. Ramosgallardo, A. Vegas, Zeit. Kristallogr. 210 (1995) 1.
[26] C.L. Condron, S.M. Kauzlarich, Inorg. Chem. 46 (2007) 2556.
[27] C.L. Condron, S.M. Kauzlarich, T. Ikeda, G.J. Snyder, F. Haarmann, P. Jeglic, Inorg. Chem. 47 (2008) 8204.
[28] F. Gascoin, S. Ottensmann, D. Stark, S.M. Haile, G.J. Snyder, Adv. Funct. Mater. 15 (2005) 1860.